

Feasibility of sinusoidal flux drive design of switched reluctance motor for reducing torque and input current ripples with three-Leg Inverter

Masaki Iida*, Masataka Ishihara*, Kazuhiro Umetani**, and Eiji Hiraki *

* Graduate school of natural science and technology,
Okayama University,
Okayama, Japan

** Graduate school of engineering,
Tohoku University,
Sendai, Japan

Published in: 2021 IEEE 19th International Power Electronics and Motion Control Conference (PEMC)

© 2021 IEEE. Personal use of this material is permitted. Permission from IEEE must be obtained for all other uses, in any current or future media, including reprinting/republishing this material for advertising or promotional purposes, creating new collective works, for resale or redistribution to servers or lists, or reuse of any copyrighted component of this work in other works.

DOI: 10.1109/PEMC48073.2021.9432579

Feasibility of Sinusoidal Flux Drive Design of Switched Reluctance Motor for Reducing Torque and Input Current Ripples with Three-Leg Inverter

Masaki Iida
Graduate school of natural science and
technology
Okayama University
Okayama, Japan
pk228e77@s.okayama-u.ac.jp

Takayuki Kusumi
Graduate school of natural science and
technology
Okayama University
Okayama, Japan
p75s6ovi@s.okayama-u.ac.jp

Kazuhiro Umetani
Graduate school of engineering
Tohoku University
Sendai, Japan
kazuhiro.umetani.e1@tohoku.ac.jp

Eiji Hiraki
Graduate school of natural science and
technology
Okayama University
Okayama, Japan
hiraki@okayama-u.ac.jp

Abstract—Switched reluctance motors (SRMs) are attractive for vehicle propulsion owing to their high thermal tolerance and comparatively high power density. However, conventional SRMs exhibit large torque and large input current ripples, which deteriorate the driving comfort and the battery lifespan. Furthermore, conventional SRMs require the special inverter topology with additional switching or rectifying devices, which leads to the cost-up of the driving system of the SRM. For solving these obstacles to the vehicular application, this paper proposes a novel SRM. The proposed SRM is based on magnetization with the sinusoidal phase flux waveform, whereby the torque and input current ripples are eliminated using a common three-leg inverter without deteriorating the power density. This paper presents the operating principles of the proposed SRM as well as simulation results in comparison with the conventional SRM and synchronous reluctance motor. As a result, the proposed SRM is elucidated to reduce the torque and input current ripples with the three-leg inverter. Furthermore, the proposed SRM is expected to improve the torque range and rotating speed range because of the sinusoidal flux waveform with reduced peak value. These results imply that the proposed SRM is promising for vehicle propulsion.

Keywords—input current ripple, motor drive, switched reluctance motor, synchronous reluctance motor, torque ripple

I. INTRODUCTION

Recently, researchers are investigating the application of switched reluctance motors (SRMs) to the vehicular propulsion [1]. The SRMs do not have the permanent magnets, which contributes to their high thermal tolerance and simple mechanical construction. In addition to this advantage, they are known to exhibit high power density compared with other reluctance motors such as the synchronous reluctance motors, which do not have permanent magnets. These features are attractive for vehicular application, where the thermal dissipation capability and the installation space are strictly limited. However, the preceding studies [2] also pointed out that SRMs tend to suffer from large torque ripple and large input current ripple, which deteriorates the driving comfort and damages the battery lifespan. Furthermore, SRM drive generally requires the special inverter [3], each phase of which is composed as a unidirectional full-bridge circuit as shown in

Fig. 1. Therefore, this special inverter can lead to the cost-up for additional switching or rectifying devices.

Conventionally, a number of techniques have been proposed to reduce the torque and input-current ripples. Reduction of the torque ripple was sought in many studies by optimization of the phase current waveforms and the motor geometry. For example, [4]–[23] proposed novel phase-current waveforms; [24]–[29] proposed the optimization of the motor geometry in combination with the optimization of the phase-current waveform. Reduction of the input-current ripple was sought by the optimization of the phase current waveform and the novel special inverter topologies with optimized control. For example, [30] [31] proposed novel phase-current waveforms; [32]–[34] proposed a special SRM inverter and its optimized control. However, these studies targeted at either one of the torque and input-current ripples.

Certainly, [3], [35]–[39] targeted at reduction of both the torque ripple and the input-current ripple. In [3] [35]–[37], the novel phase-current waveforms were proposed to reduce these ripples simultaneously. In [38] [39], further optimization of the motor geometry was investigated for this novel phase current waveform. However, these techniques cannot be applied with the three-leg inverter.

Meanwhile, a few techniques have reported the techniques for driving the SRMs with three-leg inverters [40] [41]. However, these techniques are not effective to reduce neither the torque and input-current ripples. Consequently, preceding techniques still have difficulties in solving all of the

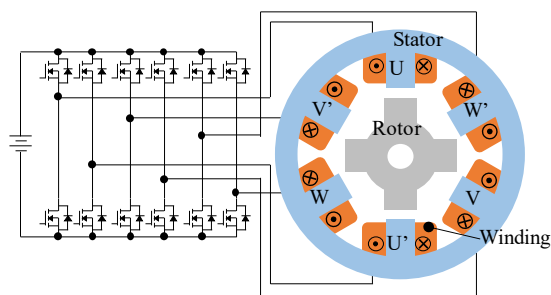


Fig. 1. Configuration of a basic three-phase concentrated-winding SRM.

three problems, i.e. the torque ripple, the input-current ripple, and the special inverter topology.

The purpose of this paper is to solve these problems by proposing a novel SRM. The proposed SRM is designed to have a sinusoidal reluctance profile, i.e. the relation between the reluctance and the electrical angle, as well as the delta-connected phase windings. As shown in this paper, the proposed SRM can eliminate the torque and input-current ripples by driving with the three-phase sinusoidal voltage supplied by the normal three-leg inverter.

Certainly, the synchronous reluctance motor (SynRMs) can also solve these three problems [42] based on the similar concept. SynRM has the sinusoidal inductance profile, i.e. the relation between the inductance and the electric angle, as well as the star-connected phase winding. The SynRM can eliminate the torque and input-current ripples by driving with the sinusoidal phase current waveform supplied by the normal three-leg inverter. However, as explained in the next section, the magnetic flux waveform of the SynRMs contains significant harmonics and has greater peak magnetic flux. As a result, SynRM tends to suffer from low power density and small maximum rotational speed, which can also be solved in the proposed SRM.

II. PROPOSED SWITCHED RELUCTANCE MOTOR

This section describes the proposed SRM in comparison with the conventional SRM, based on the three-phase concentrated-winding stator structure as depicted in Fig. 1. In this analysis, we neglect the magnetic saturation to simplify the analysis. Certainly, the SRMs can be commonly driven with the magnetic saturation of the core. However, the vehicular propulsion needs to cover a wide variety of the output torque. Therefore, the SRM can be assumed to be operated with the phase magnetic flux below the saturation level for the normal vehicle travel because the SRM should be designed to output the instantaneous large torque at the sudden acceleration or the hill start of the vehicle.

The rotor geometry of the conventional SRM has been designed so that the phase inductance profile, i.e. the dependence of the phase inductance on the electric angle, has the triangular waveform as illustrated in Fig. 2. The phase current of the conventional SRM is ideally given as the square waveform, whose top ranges for 120° in the electric angle, and the current of each phase is given with the 120° phase shift.

As widely known, the instantaneous torque τ equals to partial derivative of co-energy E_{co} of the motor with respect to the mechanical angle of rotor θ_M as

$$\tau = \frac{\partial E_{co}}{\partial \theta_M}, \quad (1)$$

Co-energy E_{co} can be expressed as follows if we approximate that the magnetic coupling between the phases is ignorable.

$$E_{co} = \sum_{k=U,V,W} \frac{1}{2} L_k (\theta_E) i_k^2, \quad (2)$$

where L is the phase inductance, i is the phase current, k is the index of the phases, and θ_E is the electric angle. The origin of

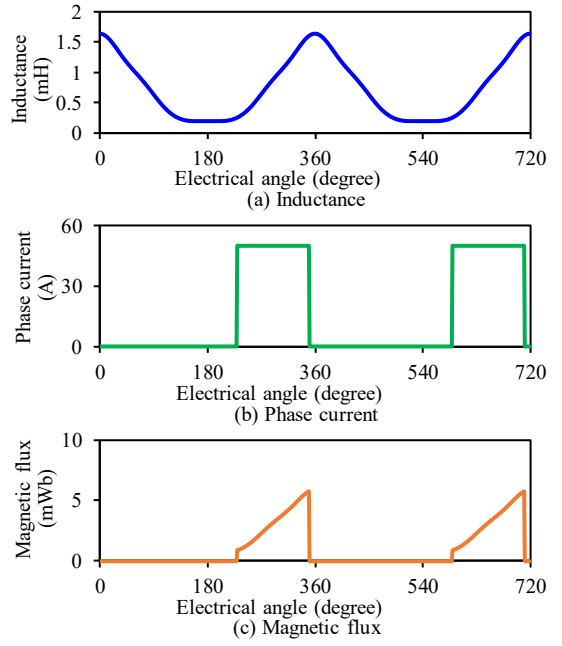


Fig. 2. Operation waveforms of the conventional SRM.

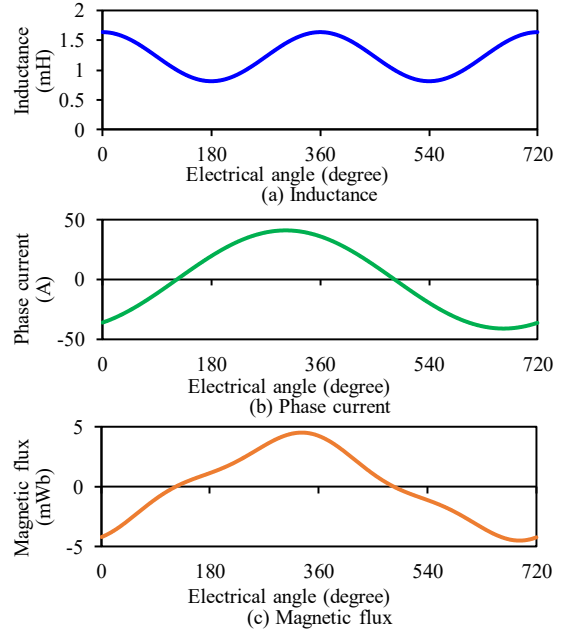


Fig. 3. Operation waveforms of the SynRM.

θ_E is set at the aligned position of phase U. Consequently, τ is formulated as follows using θ_E by substituting (2) into (1):

$$\tau = \sum_{k=U,V,W} \frac{P}{2} \frac{\partial L_k}{\partial \theta_E} i_k^2, \quad (3)$$

where P is the number of the rotor pole pairs.

Meanwhile, the input current i_{in} can be obtained as the instantaneous output power of the inverter divided by the DC bus voltage if we neglect the input current ripple caused by the switching operation, which is assumed to be decoupled by the input smoothing capacitor of the DC voltage source. Therefore we have

$$i_{in} = \frac{1}{V_{dc}} \sum_{k=U,V,W} v_k i_k, \quad (4)$$

where v_k is the output voltage of phase k . (The ripples in v_k caused by the switching operation is assumed to be decoupled.) According to Faraday's law, v_k equals to the time derivative of the flux linkage of the phase winding. Noting that the flux linkage of phase k equals to $L_k i_k$, v_k can be expressed as

$$v_k = \frac{dL_k i_k}{dt}. \quad (5)$$

Because L_k is only dependent on the electric angle θ_E , i_{in} can be obtained as follows by substituting (5) into (4):

$$\begin{aligned} i_{in} &= \frac{1}{V_{dc}} \sum_{k=U,V,W} \frac{dL_k i_k}{dt} i_k \\ &= \frac{\Omega}{V_{dc}} \sum_{k=U,V,W} \left(\frac{dL_k}{d\theta_M} i_k^2 + L_k \frac{di_k}{d\theta_M} i_k \right) \\ &= \frac{\Omega}{V_{dc}} \sum_{k=U,V,W} \left(P \frac{\partial L_k}{\partial \theta_E} i_k^2 + P \frac{L_k}{2} \frac{di_k^2}{d\theta_E} \right) \\ &= \frac{\Omega}{V_{dc}} \sum_{k=U,V,W} \left(2\tau + \frac{P}{2} L_k \frac{di_k^2}{d\theta_E} \right), \end{aligned} \quad (6)$$

where Ω is the angular velocity $d\theta_M/dt$.

As can be seen in (4), the constant phase current generates the constant instantaneous torque at a constant slope of the inductance. Hence, the total output torque of the conventional SRM is expected to be constant. In addition, according to (6), the input current i_{in} is also expected to be constant during the major part of the electric angle range of magnetization, where phase current takes a constant value. However, the conventional SRM generates large magnetic flux at the pole alignment position, which results in the long transient time for demagnetizing the phase. During this transient time of each phase, sharp spike of the input current ripple occurs due to large $L_k di_k^2/d\theta_E$, which will damage the in-vehicle battery that supplies the energy to the propulsion motor. Furthermore, this transient time also increase the torque ripple. This is the reason why the conventional SRM generates large torque ripple and large input current ripple. This problem is particularly serious in high speed operation because the transient time takes a significant portion of the switching period.

These drawbacks can be avoided by designing the phase inductance L_k and the phase current i_k to have the sinusoidal waveform, as shown in Fig. 3. In this design, the phase current i_k has half the frequency as the phase inductance L_k . For example, L_U and i_U can be expressed as

$$L_U(\theta_E) = S_0 - S_1 \cos 2\theta_E, \quad i_U = A_1 \cos(\theta_E - \alpha), \quad (7)$$

where S_0, S_1, A_1, α are constant real numbers and θ_E is the electrical angle. As a result, the harmonics of multiples of three can be eliminated from $\partial L_U/\partial \theta_E \cdot i_U^2$ and $L_U di_U^2/d\theta_E$. Therefore, the instantaneous torque τ and the input current i_{in} take constant values regardless to θ_E , because of the constant

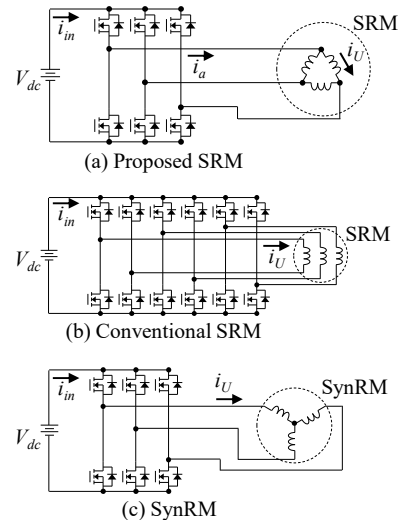


Fig. 4. Phase winding connection and driving systems of the proposed SRM, conventional SRM, and SynRM.

phase shift of 120° among the three phases. Furthermore, this design can utilize the three-leg inverter to supply the sinusoidal phase current, if the phase winding is connected in the star connection, as shown in Fig. 4(c).

This design is generally called as the synchronous reluctance motor (SynRM) [42]. This design is beneficial in eliminating both the torque and input current ripples if operated with the phase flux below the magnetic saturation level. However, the phase flux waveform significantly contains the 3rd harmonics as depicted in Fig. 3 because the phase flux ϕ_k is expressed as $\phi_k = L_k i_k / N$, where N is the number of turns of the winding per stator pole. Therefore, the phase flux waveform has a large peak and a large slope, which limits the maximum output torque and the maximum rotating speed.

The proposed SRM aims at avoiding the torque and input current ripples by designing the phase reluctance R_k and the phase flux ϕ_k to have the sinusoidal waveform, as shown in Fig. 5. In this design, R_U and ϕ_U can be expressed as

$$R_U(\theta_E) = T_0 - T_1 \cos 2\theta_E, \quad \phi_U = B_1 \cos(\theta_E - \beta), \quad (8)$$

where T_0 and T_1 are Fourier coefficients given by a motor; B_1 and β are parameters characterizing the phase magnetic flux waveform.

Because R_k and ϕ_k are expressed as $R_k = N^2/L_k$ and $\phi_k = L_k i_k / N$, (3) and (6) can be rewritten as

$$\tau = - \sum_{k=U,V,W} \frac{P}{2} \frac{\partial R_k}{\partial \theta} \phi_k^2, \quad (9)$$

$$i_{in} = \frac{\Omega}{V_{dc}} \sum_{k=U,V,W} \left(2\tau + \frac{P}{2} R_k \frac{d\phi_k^2}{d\theta} \right). \quad (10)$$

Therefore, the proposed SRM, i.e. the sinusoidal reluctance waveform design with sinusoidal phase flux drive, also results in the absence of both the input current and torque ripples if operated with the phase flux below the magnetic saturation level. Contrary to the SynRM, this design has the sinusoidal phase flux waveform, which can have a smaller

slope and therefore can be driven at higher rotational speed than the conventional SRM and the SynRM.

Meanwhile, the phase current of the proposed SRM is comprised of the fundamental wave and the 3rd harmonics. In fact, noting that $Ni_k=R_k\phi_k$, we obtain

$$i_U(\theta_E) = \frac{R_U(\theta_E)\phi_U}{N} = -\frac{B_1T_1 \cos(3\theta_E + \beta)}{2N} + \frac{2B_1T_0 \cos(\theta_E + \beta)}{2N} - \frac{B_1T_1 \cos(\theta_E - \beta)}{2N}. \quad (11)$$

Because of the 3rd harmonics contained in the phase current waveform, the three-leg inverter cannot be utilized if the three phase windings are connected in the star connection, which is the common structure of many motors including the synchronous reluctance motors. Instead, the three phase windings should however be connected in the delta connection, as illustrated in Fig. 4(a), because of the sinusoidal flux waveform. The delta connection enables the three-leg inverter to be utilized to drive this motor.

In general, the inverter can supply only the current without the harmonics of the multiples of the three to the motors with the delta connection. Therefore, all the harmonics of the multiples of three contained in the phase current must flow through the three phase windings as the circulating current. Consequently, the inverter supplies only the sinusoidal current to the proposed SRM, which is similar to many conventional synchronous motors including the SynRM. This enables many motor drive control to be applied to the proposed SRM.

The delta connection has been commonly avoided in the SynRM because this connection can induce the undesired circulating current flowing through the three phase windings and deteriorates the efficiency. In fact, as we have seen above, the circulating current must also flow in the proposed SRM. However, contrary to the SynRM, this circulating current is an important contributor to the torque output in the proposed SRM. In the SynRM with the delta-connection, the circulating current is undesired but induced because the phase flux

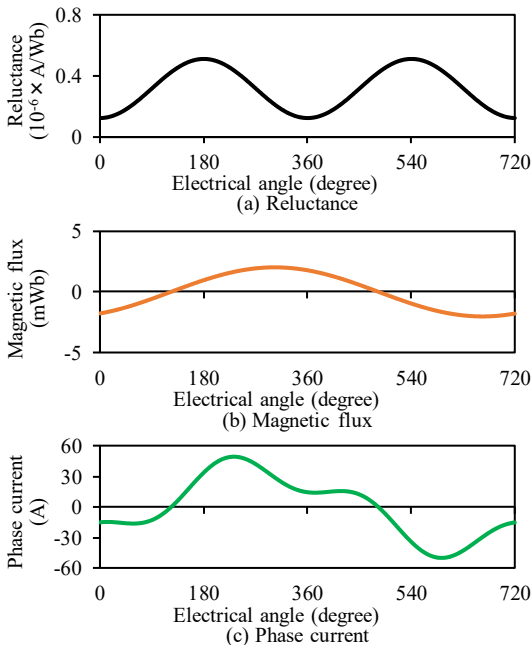


Fig. 5. Operation waveforms of the proposed SRM.

waveform contains the 3rd harmonics and therefore the undesired deviation of the phase flux waveform must occur to fit the voltage induction of the phase winding to the delta connection. (The sum of the voltage induction in the three phase windings must be zero in the delta connection.) As a result, undesired current flows through the phase windings, which deforms the sinusoidal phase current waveform. Meanwhile, in the proposed SRM, the circulating current is a natural consequence for achieving the sinusoidal phase flux waveform. Therefore, the circulating current is necessary and should not be regarded to be problematic. Consequently, the proposed SRM can solve the aforementioned three problems, i.e. the input current ripple, the torque ripple, and the special inverter.

III. SIMULATION

The simulation was performed to evaluate the operation and performance of the proposed SRM in comparison with the conventional SRM and the SynRM. For this purpose, the magnetic analysis model was constructed in the model space of the electromagnetic simulator JMAG18.1 (JSOL Corp.). Then, the circuit behavior model was constructed based on the simulation result of JMAG18.1. The circuit behavior model was applied to the circuit simulator PSIM11.1 (Myway Corp.) to evaluate the torque and input current ripples, as well as the phase current waveforms in the motor drive system shown in Fig. 4. In this comparison, we considered that all motors comprise the same stator core. Hence, the difference between these motors is assumed to lie only in the rotor shape. The materials used in the simulation model are listed in Table I.

TABLE I. MATERIAL USED IN FEM MODEL

Component	Material name or relative magnetic permeability
Stator	Material name: 35H300 (Nippon Steel Corp.)
Rotor	Material name: 35H300 (Nippon Steel Corp.)
Winding	Relative magnetic permeability: 1
Shaft	Relative magnetic permeability: 1

TABLE II. SPECIFICATIONS OF CONVENTIONAL SRM

Model number	RB165SR-96CSR (Motion System Tech. Inc.)
Rated value	1.2 kW, 96 V, 6000 r/min
Structure	Stator: 12 poles, Rotor: 8 poles, Number of turns: 14 turns/pole Outer diameter of stator: 136 mm Outer diameter of rotor: 83 mm Gap between stator and rotor: 0.3 mm Diameter of shaft: 25 mm Stack length: 40 mm
Material	35H300 (Nippon Steel Corp.)
Characteristics	Maximum reluctance R_{max} : 0.98×10^6 A/Wb (Minimum inductance: 0.2 mH) Minimum reluctance R_{min} : 0.13×10^6 A/Wb (Maximum inductance: 1.5 mH)

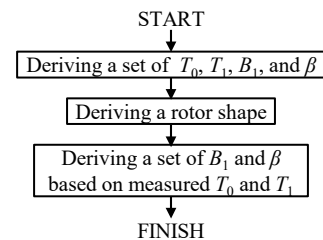


Fig. 6. Designing process employed for simulation.

A. Motor Modeling

This subsection describes the motor models of the proposed SRM and the SynRM. These models were constructed based on the simulation model of the commercially available SRM, which is regarded as the conventional SRM. The specifications of this conventional SRM are listed in Table II. Hereafter, the design procedure of these models are described in detail for the proposed SRM, although the same procedure was taken also for the SynRM.

The design procedure of the models is summarized in Fig. 6. The first step searches for the best set of parameters of T_0 , T_1 , B_1 , and β , by regarding these parameters are flexible. The second step determines the rotor shape based on the searched set of T_0 and T_1 . The third step extracts T_0 and T_1 again from the reluctance profile calculated for the designed rotor shape and then determines the current waveform.

1) Search for Parameter Set

The first step searches for a set of parameters of T_0 , T_1 , B_1 , and β under the requirement condition of Table III. In search for the parameter set, restrictions are introduced for the reluctance and the average torque.

As for the reluctance, the values at the aligned position and the unaligned position are restricted. Because the minimum gap between the stator and the rotor has been already minimized in the conventional SRM, we cannot achieve smaller reluctance for the proposed SRM. Therefore, the reluctance at the aligned position is restricted to be equal or greater than that of the conventional SRM. Similarly, the rotor shape of the conventional SRM is commonly designed to have as large reluctance at the unaligned position as possible, we cannot expect to have larger reluctance for the proposed SRM. Therefore, the reluctance at the unaligned position is restricted to be equal or less than that of the conventional SRM.

As for the average torque, the average torque τ_{ave} for performance comparison was set at 1 N·m, where the conventional SRM is hardly affected by effect of the magnetic saturation. The average torque τ_{ave} was calculated by

$$\tau_{ave} = \frac{3P}{4} B_1^2 T_1 \sin 2\beta, \quad (12)$$

The search for the parameter set was performed so that the torque per copper loss ratio is maximized satisfying the other criteria. The copper loss P_{copper} was calculated by

$$P_{copper} = 3i_{U_rms}^2 r_{on}, \quad (13)$$

where i_{U_rms} is the effective value of the phase current; r_{on} is the winding resistance, i.e. 0.05 Ω . (Note that the copper loss generated between the inverter and the SRM is comparatively small and therefore the loss is neglected.)

Finally, the parameters were determined as Table IV.

TABLE III. DERIVATION CONDITION EMPLOYED FOR DESIGN

Criteria	Value
Average Torque	1 N·m
Reluctance at Aligned Position	\geq Conventional design
Reluctance at Unaligned Position	\leq Conventional design
Torque per Copper Loss Ratio	Maximum

2) Determination of Rotor Shape

Based on the determined parameters set, the second step determines the rotor shape using JMAG18.1 (JSOL Corp.).

For determining the optimum rotor shape, this step approximates the rotor shape by a 288-gon, as presented in Fig. 7(a). The rotor shape was determined by searching for the optimum distance between each vertex and the outline of the inner diameter of the stator core that best fits the designed reluctance waveform derived in the first step.

First, D_{18} , D_{54} , D_{90} , D_{126} , D_{162} , D_{198} , D_{234} , and D_{270} are determined. In this subsection, vertex-18, vertex-54, vertex-90, vertex-126, vertex-162, vertex-198, vertex-234, and vertex-270 are regarded as the farthest vertexes from the inner diameter of the stator. Therefore, D_{18} , D_{54} , D_{90} , D_{126} , D_{162} , D_{198} , D_{234} , and D_{270} are determined so that the inductance measured by finite-element-method achieves the maximum reluctance of the designed reluctance waveform.

Second, D_0 , D_{36} , D_{72} , D_{108} , D_{144} , D_{180} , D_{216} , and D_{252} are determined. Vertex-0, vertex-36, vertex-72, vertex-108, vertex-144, vertex-180, vertex-216, and vertex-252 are regarded as the closest vertexes to the inner diameter of the stator. Therefore, D_0 , D_{36} , D_{72} , D_{108} , D_{144} , D_{180} , D_{216} , and D_{252} are set to the minimum gap of the conventional design SRM, i.e. 0.3 mm.

Third, the other vertexes are determined. To make the reluctance profile to be a sinusoidal waveform, the vertexes are determined so that the D_n changes sinusoidally as

$$D_n = \frac{D_{18} + D_0}{2} - \frac{D_{18} - D_0}{2} \cos\left(8n \frac{2\pi}{288}\right), \quad (14)$$

where n is an integer and $0 \leq n \leq 287$. As a result, the rotor shape was determined as presented in Fig. 7(b).

3) Determination of Phase Current Waveform

The third step derived the phase current waveform again based on the reluctance profile of the rotor shape obtained in

TABLE IV. PARAMETERS DERIVED IN FIRST STEP

Parameter	Value	Parameter	Value
T_0	0.26×10^6 A/Wb	T_1	-0.13×10^6 A/Wb
$R_U(0)$	0.13×10^6 A/Wb	$R_U(\pi/2)$	0.39×10^6 A/Wb
B_1	1.58 mWb	β	-45 degrees

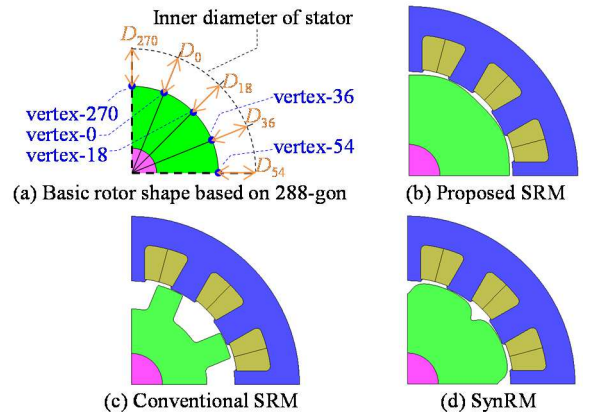


Fig. 7. Rotor shape employed for simulation.

the second step. The result is shown in Fig. 8. Figure 8 also shows the inductance, the reluctance, the phase current, and the phase flux of all the three motor models, i.e. the proposed SRM, the conventional SRM, and the SynRM.

The conventional SRM is assumed to be driven by the ideal square wave phase current. This square wave phase current was parameterized by the firing angle θ_{on} , extinction angle θ_{off} , and the peak current I_{peak} under the condition of $\theta_{off} - \theta_{on} = 120^\circ$. These parameters were tuned depending on rotating speed and output torque to maximize the torque per copper loss ratio at 1000 r/min.

The SynRM was designed by the same design procedure as the proposed SRM based on the formulae for the SynRM. The rotor shape was designed as in Fig. 7(d). The only difference in the design procedure from the proposed SRM is that the distance of vertexes from the inner diameter of the stator core should be designed to form the inverted sinusoidal waveform because the inductance changes sinusoidally. Therefore, the vertexes of the SynRM are determined according to

$$\frac{1}{D_n} = \frac{D_{18} + D_0}{2D_0D_{18}} + \frac{D_{18} - D_0}{2D_0D_{18}} \cos\left(8n \frac{2\pi}{288}\right). \quad (15)$$

B. Torque and Input Current Ripple

Based on the electromagnetic analysis results shown in the previous subsection, the behavior model of the motors were constructed for the circuit simulation by PSIM11.1. By utilizing this behavior model, the motor drive system shown in Fig. 4 were constructed for the simulation. The conventional SRM was connected to the three-phase H-bridge inverter; the proposed SRM and the SynRM were connected to three-leg inverter. Each motor model in the simulation circuit comprised the inductance profile in Fig. 8(a). Each inverter was supplied with the DC bus voltage of $V_{dc} = 96$ V. The inverter output current was controlled to track the current command value shown in Fig. 8(c) using the hysteresis control. Hence, the output torque was set at 1 N·m. The hysteresis width was set at 2 A.

The waveforms were obtained at the rotating speed of 1000 r/min. The rotating speed of 1000 r/min is a typical speed of the vehicle propulsion motors and therefore beneficial to

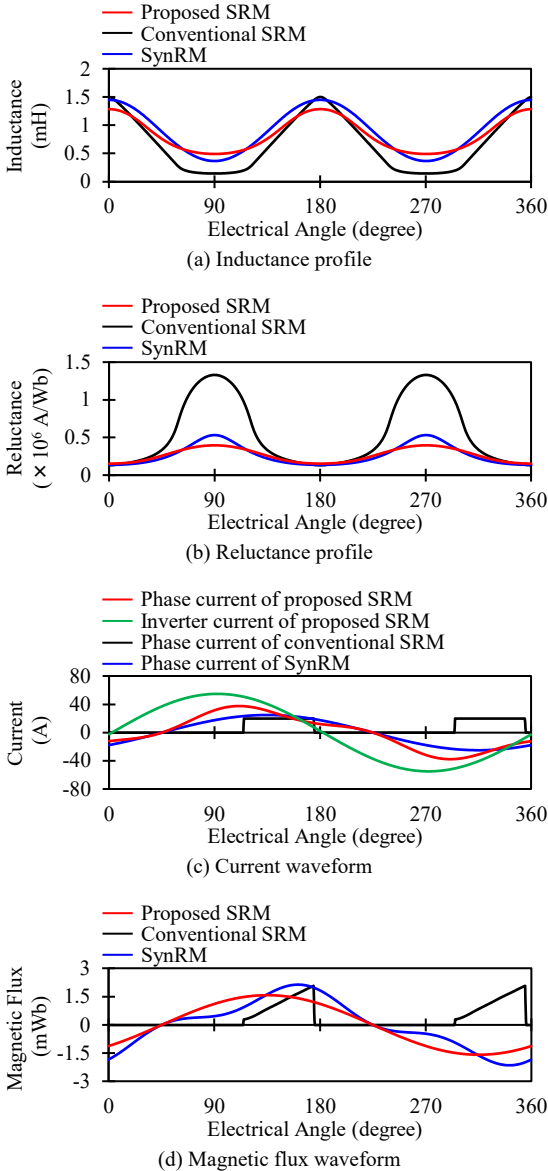


Fig. 8. Designed inductance/reluctance profile, phase current waveform, phase flux waveform of proposed SRM, conventional SRM, and SynRM.

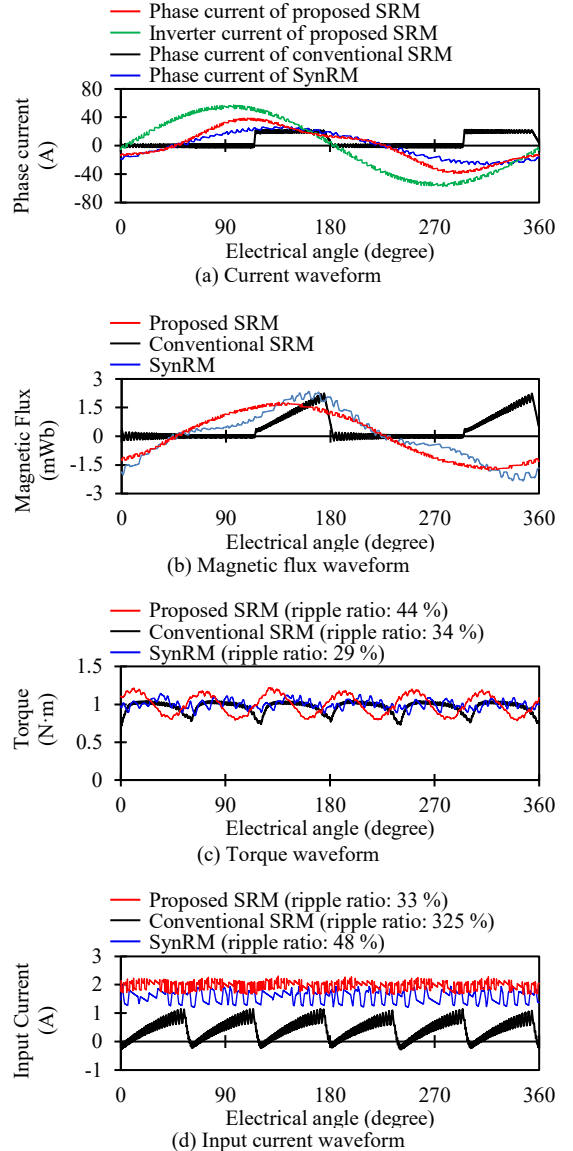


Fig. 9. Simulation results at 1000 r/min.

discuss the operating waveforms because the DC bus voltage is enough high to track the current waveforms.

Figure 9(a) presents the current waveforms. Although the phase current of the proposed SRM contained the 3rd harmonics, the inverter output current did not contain any harmonics, as well as the SynRM. This result revealed that the proposed SRM can be driven by the three-leg inverter.

Figure 9(b) presents the magnetic flux waveform. The waveform contributed by the proposed SRM did not contain harmonics and the peak-to-peak value was the smallest. In other words, the proposed SRM had the largest margin of the magnetic flux to the magnetic saturation level among the other motors. Therefore, this result implies that the proposed SRM can achieve the wide torque range and rotating speed range.

Figures 9(c) and 9(d) present the torque waveforms and the input current waveforms. The ripple ratios, which are defined as a peak-to-peak value normalized by the average value, are displayed on the legends of Figs. 9(c) and 9(d). The proposed SRM suppressed the torque ripple, similarly as the other motors. Furthermore, the proposed SRM effectively suppressed the input current ripple as the SynRM. Certainly, small ripples remained in the torque and input current waveforms. Although the reason is not clarified in this paper, the ripples may be caused by the harmonics remaining in the reluctance profile of the proposed SRM in Fig. 8(b). Therefore, by searching the rotor shape with more advanced optimization technique, the ripples will be further reduced. Nonetheless, these results revealed the effective suppression of the torque ripple and the input current ripple by the proposed SRM.

It should be noted that the phase-current of the proposed SRM was greater than those of the others, resulting in more copper loss than the other motors. Nonetheless, as presented in Fig. 9(b), the amplitude of the magnetic flux waveform of the proposed SRM was less than the other motors and the magnetic flux waveform of the proposed SRM did not contain harmonics. This result implies that the proposed SRM generates less core loss than the other motors. Therefore, the motor loss of the proposed SRM may not be necessarily larger than the other motors in extremely high speed operation. However, the reduction technique of the phase-current is important topic to be addressed in future researches.

C. High Speed Operation

Next, we compared the high speed operation among the proposed SRM, the conventional SRM and the SynRM. For

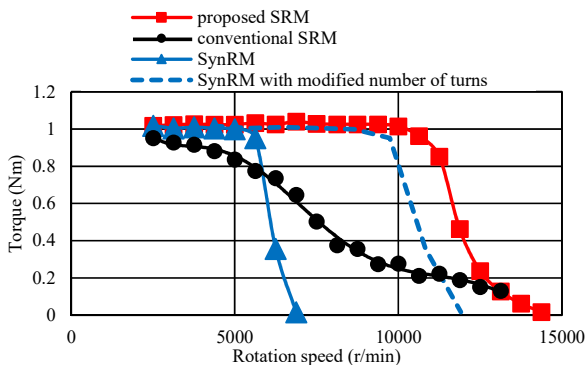


Fig. 10. Simulation result of torque-speed characteristic. SynRM with modified number of turns indicates estimation of SynRM having phase winding with $1/\sqrt{3}$ times as much number of turns as the proposed SRM and driven with $\sqrt{3}$ times as large phase current command value as SynRM.

this purpose, we simulated the torque output of the motor driving systems at various rotation speed under the phase current command value of Fig. 8(c), which indicates 1 N·m torque. The DC bus voltage of the inverter was set at 96V. The inverter output current was controlled by the hysteresis control with the hysteresis width of 2 A.

The result is shown in Fig. 10. The result revealed remarkable improvement in the torque-speed characteristic by the proposed SRM compared to the conventional SRM and the SynRM. Certainly, it should be noted that comparison between the proposed SRM and the SynRM is unfair if compared under the same number of turns of the phase winding as in Fig. 10, because the proposed SRM has the delta-connection and the SynRM has the star-connection.

However, the result in Fig. 10 shows that the proposed SRM exhibits still better torque-speed characteristic than SynRM, even if the SynRM has $1/\sqrt{3}$ times as much number of turns as the proposed SRM and is driven with $\sqrt{3}$ times as large phase current command value as the SynRM of Fig. 8(c). In this case, the torque of this SynRM will drop at $\sqrt{3}$ times as high rotational speed as the result of the SynRM in Fig. 10. Therefore, the SynRM with the modified number of turns and phase current command value is expected to exhibit the torque-speed characteristic shown in the dashed line in Fig. 10. Consequently, this result implies that the proposed SRM can improve the rotation speed range compared to the SynRM.

IV. CONCLUSIONS

The conventional SRM is attractive for comparatively high power density, although this motor has severe drawbacks of (I) large torque ripple, (II) large input current ripple, and (III) need of the special inverter topology, which hindered the application of this motor to the vehicle propulsion. To overcome these drawbacks, this paper proposed a novel SRM driven by the sinusoidal phase flux. The simulation successfully supported the operating principle that solved these three drawbacks. Furthermore, the simulation also revealed that the proposed SRM is expected to achieve wider torque and rotation speed range than SynRM because the proposed SRM can be driven by the small amplitude of the magnetic flux and does not contain harmonics in the magnetic flux waveform. These results supported the feasibility of the proposed SRM, although reduction in the copper loss will be an important issue to be addressed in future researches.

REFERENCES

- [1] Z. Q. Zhu and C. C. Chan, "Electrical machine topologies and technologies for electric, hybrid, and fuel cell vehicles," in Proc. IEEE Vehicle Power Propulsion Conf., Harbin, China, pp. 1–6, Sept. 2008.
- [2] W. Suppharangsarn and J. Wang, "Experimental validation of a new switching technique for DC-link capacitor minimization in switched reluctance machine drives," in Proc. IEEE Int. Electric Machines Drives Conf., Chicago, USA, pp. 1031–1036, May 2013.
- [3] T. Kusumi, T. Hara, K. Umetani, and E. Hiraki, "Phase-current waveform for switched reluctance motors to eliminate input-current ripple and torque ripple in low-power propulsion below magnetic saturation," IET Power Electronics, vol. 13, no. 15, pp. 3351–3359, Nov. 2020.
- [4] I. Husain and M. Ehsani, "Torque ripple minimization in switched reluctance motor drives by PWM current control," IEEE Trans. Power Electron., vol. 11, no. 1, pp. 83–88, Jan. 1996.
- [5] M. Rodrigues, P. J. Costa Branco, and W. Suemitsu, "Fuzzy logic torque ripple reduction by turn-off angle compensation for switched reluctance motors," IEEE Trans. Ind. Electron., vol. 48, no. 3, pp. 711–715, June 2001.

- [6] I. Husain, "Minimization of torque ripple in SRM drives," *IEEE Trans. Ind. Electron.*, vol. 49, no. 1, pp. 28-39, Feb. 2002.
- [7] L. O. A. P. Henriques, P. J. Costa Branco, L. G. B. Rolim, and W. I. Suemitsu, "Proposition of an offline learning current modulation for torque-ripple reduction in switched reluctance motors: design and experimental evaluation," *IEEE Trans. Ind. Electron.*, vol. 49, no. 3, pp. 665-676, June 2002.
- [8] P. L. Chapman and S. D. Sudhoff, "Design and precise realization of optimized current waveforms for an 8/6 switched reluctance drive," *IEEE Trans. Power Electron.*, vol. 17, no. 1, pp. 76-83, Jan. 2002.
- [9] C. Mademlis and I. Kioskeridis, "Performance optimization in switched reluctance motor drives with online commutation angle control," *IEEE Trans. Energy Conversion*, vol. 18, no. 3, pp. 448-457, Sept. 2003.
- [10] N. T. Shaked and R. Rabinovici, "New procedures for minimizing the torque ripple in switched reluctance motors by optimizing the phase-current profile," *IEEE Trans. Magn.*, vol. 41, no. 3, pp. 1184-1192, Mar. 2005.
- [11] X. D. Xue, K. W. E. Cheng, and S. L. Ho, "Optimization and evaluation of torque-sharing functions for torque ripple minimization in switched reluctance motor drives," *IEEE Trans. Power Electron.*, vol. 24, no. 9, pp. 2076-2090, Sept. 2009.
- [12] D. H. Lee, J. Liang, Z. G. Lee, and J. W. Ahn, "A simple nonlinear logical torque sharing function for low-torque ripple SR drive," *IEEE Trans. Ind. Electron.*, vol. 56, no. 8, pp. 3021 - 3028, Aug. 2009.
- [13] X. D. Xue, K. W. E. Cheng, J. K. Lin, Z. Zhang, K. F. Luk, T. W. Ng, and N. C. Cheung, "Optimal control method of motoring operation for srm drives in electric vehicles," *IEEE Trans. Vehicular Tech.*, vol. 59, no. 3, pp. 1191-1204, Mar. 2010.
- [14] V. P. Vujčić, "Minimization of torque ripple and copper losses in switched reluctance drive," *IEEE Trans. Power Electron.*, vol. 27, no. 8, pp. 388-399, Jan. 2012.
- [15] C. Moron, A. Garcia, E. Trempts, and J. A. Somolinos, "Torque control of switched reluctance motors," *IEEE Trans. Magn.*, vol. 48, no. 4, pp. 1661-1664, Apr. 2012.
- [16] R. Mikail, I. Husain, Y. Sozer, M. S. Islam, and T. Sebastian, "Torque-ripple minimization of switched reluctance machines through current profiling," *IEEE Trans. Ind. Appl.*, vol. 49, no. 3, pp. 1258-1267, May 2013.
- [17] J. Ye, B. Bilgin, and A. Emadi, "An offline torque sharing function for torque ripple reduction in switched reluctance motor drives," *IEEE Trans. Energy Conversion*, vol. 30, no. 2, pp. 726-735, June 2015.
- [18] J. Ye, B. Bilgin, and A. Emadi, "An extended-speed low-ripple torque control of switched reluctance motor drives," *IEEE Trans. Power Electron.*, vol. 30, no. 3, pp. 1457-1470, Mar. 2015.
- [19] P. Dúbravka, P. Rafajdus, P. Makyš, and L. Szabó, "Control of switched reluctance motor by current profiling under normal and open phase operating condition," *IET Electric Power Appl.*, vol. 11, no. 4, pp. 548-556, Apr. 2017.
- [20] T. Kusumi, T. Hara, K. Umetani, and E. Hiraki, "Theoretical Derivation of Phase Current Profile for Switched Reluctance Motors to Suppress Radial Force Ripple and Torque Ripple," in *Proc. 2018 IEEE 27th International Symposium on Industrial Electronics (ISIE)*, Cairns, QLD, Australia, pp. 1037-1042 June 2018.
- [21] M. Kawa, K. Kiyota, J. Furqani, and A. Chiba, "Acoustic noise reduction of a high-efficiency switched reluctance motor for hybrid electric vehicles with novel current waveform," *IEEE Trans. Ind. Appl.*, vol. 55, no. 3, pp. 2519-2528, May 2019.
- [22] H. Li, B. Bilgin, and A. Emadi, "An improved torque sharing function for torque ripple reduction in switched reluctance machines," *IEEE Trans. Power Electron.*, vol. 34, no. 2, pp. 1635-1644, Feb. 2019.
- [23] T. Husain, A. Elrayah, Y. Sozer, and I. Husain, "Unified control for switched reluctance motors for wide speed operation," *IEEE Trans. Ind. Electron.*, vol. 66, no. 5, pp. 3401-3411, May 2019.
- [24] N. K. Sheth and K. R. Rajagopal, "Optimum pole arcs for a switched reluctance motor for higher torque with reduced ripple," *IEEE Trans. Magn.*, vol. 39, no. 5, pp. 3214-3216, Sept. 2003.
- [25] J. W. Lee, H. S. Kim, B. I. Kwon, and B. T. Kim, "New rotor shape design for minimum torque ripple of SRM using FEM," *IEEE Trans. Magn.*, vol. 40, no. 2, pp. 754-757, Mar. 2004.
- [26] N. K. Sheth and K. R. Rajagopal, "Torque profiles of a switched reluctance motor having special pole face shapes and asymmetric stator poles," *IEEE Trans. Magn.*, vol. 40, no. 4, pp. 2035-2037, Jul. 2004.
- [27] Y. K. Choi, H. S. Yoon, and C. S. Koh, "Pole-shape optimization of a switched-reluctance motor for torque ripple reduction," *IEEE Trans. Magn.*, vol. 43, no. 4, pp. 1797-1800, Apr. 2007.
- [28] G. Li, J. Ojeda, S. Hlioui, E. Hoang, M. Lecrivain, and M. Gabsi, "Modification in rotor pole geometry of mutually coupled switched reluctance machine for torque ripple mitigating," *IEEE Trans. Magn.*, vol. 48, no. 6, pp. 2025-2034, June 2012.
- [29] B. Anvari, H. A. Toliyat, and B. Fahimi, "Simultaneous optimization of geometry and firing angles for in-wheel switched reluctance motor drive," *IEEE Trans. Transportation Electrification*, vol. 4, no. 1, pp. 322-329, Mar. 2018.
- [30] C. R. Neuhaus, N. H. Fuengwarodsakul, and R. W. De Doncker, "Control scheme for switched reluctance drives with minimized DC-link capacitance," *IEEE Trans. Power Electron.*, vol. 23, no. 5, pp. 2557-2564, Sept. 2008.
- [31] W. Suppharangsarn, and J. Wang, "Switching technique for minimisation of DC-link capacitance in switched reluctance machine drives," *IET Elect. Syst. Transportation*, vol. 5, no. 4, pp. 185-193, Dec. 2015.
- [32] F. Yi and W. Cai, "A quasi-Z-source integrated multiport power converter as switched reluctance motor drives for capacitance reduction and wide-speed-range operation," *IEEE Trans. Power Electron.*, vol. 31, no. 11, pp. 7661-7676, Nov. 2016.
- [33] W. Cai and F. Yi, "An integrated multiport power converter with small capacitance requirement for switched reluctance motor drive," *IEEE Trans. Power Electron.*, vol. 31, no. 4, pp. 3016-3026, Apr. 2016.
- [34] F. Yi and W. Cai, "Modeling, control, and seamless transition of the bidirectional battery-driven switched reluctance motor/generator drive based on integrated multiport power converter for electric vehicle," *IEEE Trans. Power Electron.*, vol. 31, no. 10, pp. 7099-7111, Oct. 2016.
- [35] T. Kusumi, T. Hara, K. Umetani, and E. Hiraki, "Simple control technique to eliminate source current ripple and torque ripple of switched reluctance motors for electric vehicle propulsion," in *Proc. Annu. Conf. IEEE Ind. Elect. Soc. (IECON2016)*, Florence, Italy, pp. 1876-1881, Oct. 2016.
- [36] T. Kusumi, T. Hara, K. Umetani, and E. Hiraki, "Simple analytical derivation of magnetic flux profile eliminating source current ripple and torque ripple of switched reluctance motors for electric vehicle propulsion," in *Proc. IEEE Appl. Power Electron. Conf. Expo. (APEC2017)*, Tampa, FL, USA, pp. 3142-3149, Mar. 2017.
- [37] T. Kusumi, K. Kobayashi, K. Umetani, and E. Hiraki, "Analytical Derivation of Phase Current Waveform Eliminating Torque Ripple and Input Current Ripple of Switched Reluctance Motors under Magnetically Saturated Operation," in *Proc. IEEE Energy Conversion Congr. Expo. (ECCE2019)*, Baltimore, MD, USA, pp. 6540-6547, Oct. 2019.
- [38] T. Kusumi, T. Hara, K. Umetani, and E. Hiraki, "Rotor configuration which reduces copper loss of switched reluctance motors with suppression of torque ripple and input current ripple," in *Proc. IEEE Energy Conversion Congr. Expo. (ECCE2018)*, Portland, OR, USA, pp. 6097-6103, Sept. 2018.
- [39] T. Kusumi, T. Hara, K. Umetani, and E. Hiraki, "Simultaneous Tuning of Rotor Shape and Phase Current of Switched Reluctance Motors for Eliminating Input Current and Torque Ripples with Reduced Copper Loss," *IEEE Transactions on Industry Applications*, vol. 56, no. 6, pp. 6384-6398, Nov. 2020.
- [40] J.-Y. Lee, B.-K. Lee, T. Sun, J.-P. Hong, and W.-T. Lee, "Dynamic Analysis of Toroidal Winding Switched Reluctance Motor Driven by 6-Switch Converter," *IEEE Transactions on Magnetics*, vol. 42, no. 4, pp. 1275-1278, Mar. 2006.
- [41] T. Husain, Y. Sozer, and I. Husain, "DC Assisted Bipolar Switched Reluctance Machine," *IEEE Transactions on Industry Applications*, vol. 52, no. 3, pp. 2098-2109, Mar. 2017.
- [42] O. Payza, Y. Demir, and M. Aydin, "Investigation of Losses for a Concentrated Winding High-Speed Permanent Magnet-Assisted Synchronous Reluctance Motor for Washing Machine Application," *IEEE Trans. Magn.*, vol. 54, no.11, 8207606, 2018.